Faraday Discussions

Accepted Manuscript

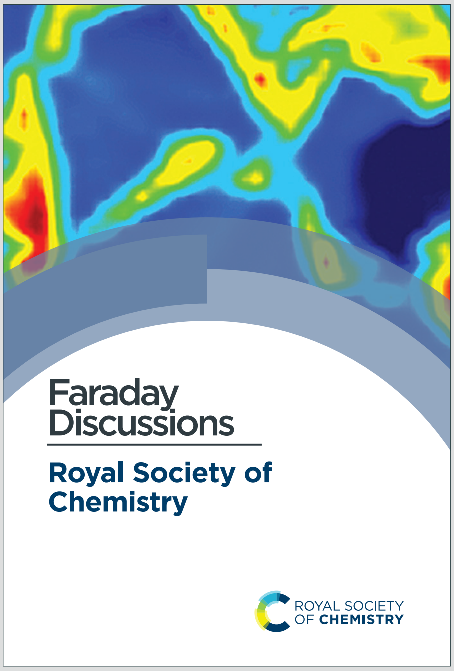

This article can be cited before page numbers have been issued, to do this please use: A. Acheche, J. Nelayah, R. Gatti, D. Alloyeau, C. Ricolleau and H. Amara, *Faraday Discuss.*, 2025, DOI: 10.1039/D5FD00096C.

View Article Online
DOI: 10.1039/D5FD00096C

Journal Name

ARTICLE TYPE

Cite this: DOI: 00.0000/xxxxxxxxxx

Received Date
Accepted Date

DOI: 00.0000/xxxxxxxxxx

Thermal stability of CoNiPtCuAu nanoalloys: from segregation to melting properties

Anissa Acheche,[a,b] Jaysen Nelayah,[b] Riccardo Gatti,[a] Damien Alloyeau,[b] Christian Ricolleau,[b] and Hakim Amara[a,b]

Recent breakthroughs in the field of high-entropy alloy nanoparticles (HEA NPs) have significantly expanded their potential applications (such as catalysis or energy storage) making them promising candidates for use over a wide temperature range. However, their thermal stabilities are not yet fully understood which is crucial to their future development. To better understand these phenomena and the underlying mechanisms, we performed molecular dynamic simulations by adopting an incremental approach to investigate the structural and thermal stability of CoNiPtCuAu HEA NP as well as their ternary and quaternary sub-alloys. More precisely, CoNiPt ternary system is first considered and then Cu and Au atoms are progressively introduced with the aim to analyse and quantify the thermal stability of HEA NPs in terms of their melting temperature and segregation mechanisms. Through our atomic-scale simulations, we demonstrate the negative impact of Au and Cu atoms on thermal stabilisation, whose presence at the surface tends to favour melting of the NPs because of their low melting point. These detailed analyses provide a robust and relevant research approach for identifying the key parameters influencing the thermal stability of HEA NPs, which is essential for obtaining such nano-objects with optimised structural and thermal properties.

1 Introduction

High-entropy alloy (HEA) materials are characterized by compositional complexities (increasing number and diversity of mixing elements) resulting in distinctive features that are attracting interest from various research and application fields. In particular, HEAs have received growing attention and have become one of the most investigated materials, for their mechanical properties[1–3]. While considerable research efforts have been devoted to bulk HEAs, recent advances in the synthesis of single-phase HEA nanoparticles (NPs) have broadened their applications in catalysis and energy-related applications[4–8]. At the nanoscale, several challenges have to be addressed starting with mastering the synthesis process. The latter has been achieved through various approaches including high-temperature methods[9–11] (carbothermal shock, plasma arc discharge and pulsed laser ablation syntheses) with varying degrees of efficiency as well as soft synthesis conditions derived from wet-chemistry approaches[12,13]. Furthermore, a crucial point for their applications is fundamental knowledge of their thermal stability, given that in the case of catalytic applications or as thermoelectric materials, the required temperature conditions are between 400 and 1400 K[14,15]. Regarding bulk HEAs, the understanding of their phase stabilities as a function of composition and temperature is scarce. This is equally true at the nanoscale where the properties of NPs differ significantly from their bulk counterparts due to their high surface-area-to-volume ratio. At the nanoscale, particle size effects should also be considered as the increased surface area provides additional degrees of freedom that significantly impact the stability of these nano-objects.

Such a high level of complexity calls for extensive studies of the phase diagram of this new class of materials where segregation effects have been shown experimentally to be activated as a function of both composition[11] and temperature[16]. For instance, pronounced structural and chemical evolutions in CoNiPtCuAu NPs have been revealed by combining *in situ* scanning transmission electron microscopy (STEM) heating and atomistic simulations. More precisely, the segregation of gold and copper, followed by their evaporation, has been observed at the surface of CoNiPtCuAu NPs annealed in vacuum at high temperature, questioning the high thermal stability generally attributed to HEA materials. The present work aims to go beyond by providing atomic-scale insight into such phenomena through the exploration of CoNiPtCuAu HEA NPs as well as their ternary and quaternary sub-alloys. This is essentially a model system whose various elements have sufficiently distinct physical properties to enable identifica-

---

[a] Université Paris-Saclay, ONERA, CNRS, Laboratoire d'Étude des Microstructures (LEM), 92322, Châtillon, France.
[b] Université de Paris, Laboratoire Matériaux et Phénomènes Quantiques (MPQ), CNRS-UMR7162, 75013 Paris, France; E-mail: hakim.amara@onera.fr

View Article Online
DOI: 10.1039/D5FD00096C

tion of the driving forces controlling the stability of the HEA NPs selected. Previous work based on Molecular Dynamics (MD) calculations has solely investigated the thermal stability of the HEA NPs, while, in some cases, highlighting segregation effects[17–19]. Herein, we adopt an incremental approach to explore the structural properties and thermal stability of CoNiPtCuAu HEA NPs. We first consider the CoNiPt ternary system at finite temperature and then progressively introduce, one by one, the segregating elements of the quinary alloy (i.e. Cu and Au) in order to assess their impact on thermal stability. Such a progressive approach, which can be generalized to other HEA nanosystems, provides a consistent research framework towards the identification of the key parameters influencing their thermal stability. This knowledge is of paramount importance for enabling the engineering of HEA NPs with optimized structural and thermal properties.

2 Segregation effects in quinary CoNiPtCuAu alloy NPs

First, we consider the thermal stability of CoNiPtCuAu HEA NPs, whose complete study is presented in Reference[16]. In the following, we briefly recall the main results and conclusions that are relevant to the present work, i.e. the case a NP adopting an icosahedral CoNiPtCuAu structure since TEM structural analysis confirmed the presence of these morphologies[16]. To investigate their structural and chemical evolution with temperature, MD simulations were performed using the open source large-scale Atomic/Molecular Massively Parallel Simulators (LAMMPS) package[20]. In particular, the Embedded Atom Method (EAM) potential derived by Zhou *et al.*[21] was employed to describe the interaction between different atomic pairs present in case of the Co-Ni-Pt-Cu-Au systems. MD calculations were based on the Verlet algorithm for integration of the equations of motion (with a time step of 1 fs including a temperature damping parameter equal to 100 time steps) coupled to the Nose-Hover thermostat in the canonical NVT ensemble. To avoid any artefacts arising from the interaction generated by periodic boundary conditions, the supercell size was made sufficiently large in all directions (100 nm).

Figure 1a depicts a typical case of the structural evolution of a 3-nm quinary Co-Ni-Pt-Cu-Au NP containing 923 atoms and with equiatomic composition as a function of temperature. The starting structure is a solid solution in which the five elements are homogeneously distributed. At low T (< 600 K), no significant structural change is observed in the NP. Above a threshold temperature (600 K), segregation phenomena are thermally activated, leading to an enrichment of Cu and Au at the surface with the NP maintaining a solid state. As the temperature is further increased, the particle melts at 1100 K, with its surface completely made up of Cu and Au atoms. From these MD calculations, it can be concluded that the thermal stability of HEA NPs is strongly controlled or even reduced by surface effects that greatly reinforce the segregation of specific elements. Note our calculations have revealed similar findings for other NP sizes (ranging from 2.1 to 5.2 nm).

It is worth critically assessing the quality and, above all, the reliability of the potential employed in the MD simulations, especially for characterizing the temperature-dependent structure of NP where numerous atomic interactions are involved. In the present work, we have selected an EAM potential developed by Zhou *et al.*[21] which is particularly used in the HEA community but has been never tested in the case of HEA NPs. For the validation of potential, we carried out comparisons with another EAM-type potential, i.e. Foiles *et al.*[22] which has been extensively employed and validated in case of the Cu-Au-Ni-Pt quaternary sub-systems, though for bulk systems. Figures 1b and c display the surface concentration for each element at different temperatures from MD simulations based on both potentials. In both cases, Au and Cu segregation increasing with the temperature, as discussed above, are numerically reproduced. Although the general trend is the same for both potentials, it can be noted that surface concentrations differ quantitatively at a given temperature. However, a simple temperature shift reveals exactly the same behavior, as shown by the evolution of Au concentration at the surface in Figure 1c. Therefore, this comparative analysis reveals that the segregation effects observed is robust and that the potential developed by Zhou *et al.* is a convincing choice for the temperature study of NP HEA.

In summary, atomic-scale simulations have shown that up to a threshold temperature, NP always adopts an HEA-type configuration with atoms in solid solution. Beyond, the presence of surfaces destabilizes the system, leading to segregation phenomena and melting of the NP. As a step further towards a better understanding and control of the phase stability and transformations of CoNiPtCuAu HEA NPs, it is essential to identify the key parameters and mechanisms driving their thermal stability.

3 Physical properties of the pure elements and NPs

In simple alloy systems such as binary alloys (surfaces or NPs), many studies have established that their structural properties are controlled by different driving forces[23]. Regarding segregation effects, three main features are commonly highlighted which are the cohesion, alloy and size effects[24–26]. In other words, the segregating element within an alloy is favoured by the lowest surface energy to minimize the free energy of the system and the largest atomic radius as the surface relaxes stresses favorably. In addition, segregation is reinforced by the tendency of the alloy to form homoatomic bonds at the expense of heteroatomic ones. Knowing the relevance of such factors, Table 1 shows the physical properties, calculated with the EAM potential used here, of each element of the quinary Cu-Au-Co-Ni-Pt alloy. The computed lattice parameters and the cohesive energies are in very good agreement with experimental or *ab initio* data. Regarding the surface energies (γ), EAM potentials lead to their underestimations, around 40 % in average. Nevertheless, these deviations do not compromise the qualitative description of the structural properties of the targeted HEA NPs and their sub-systems. Typically, the hierarchy between the surface energies of (100) and (110) surfaces, i.e. $\gamma_{111} < \gamma_{001}$,

View Article Online
DOI: 10.1039/D5FD00096C

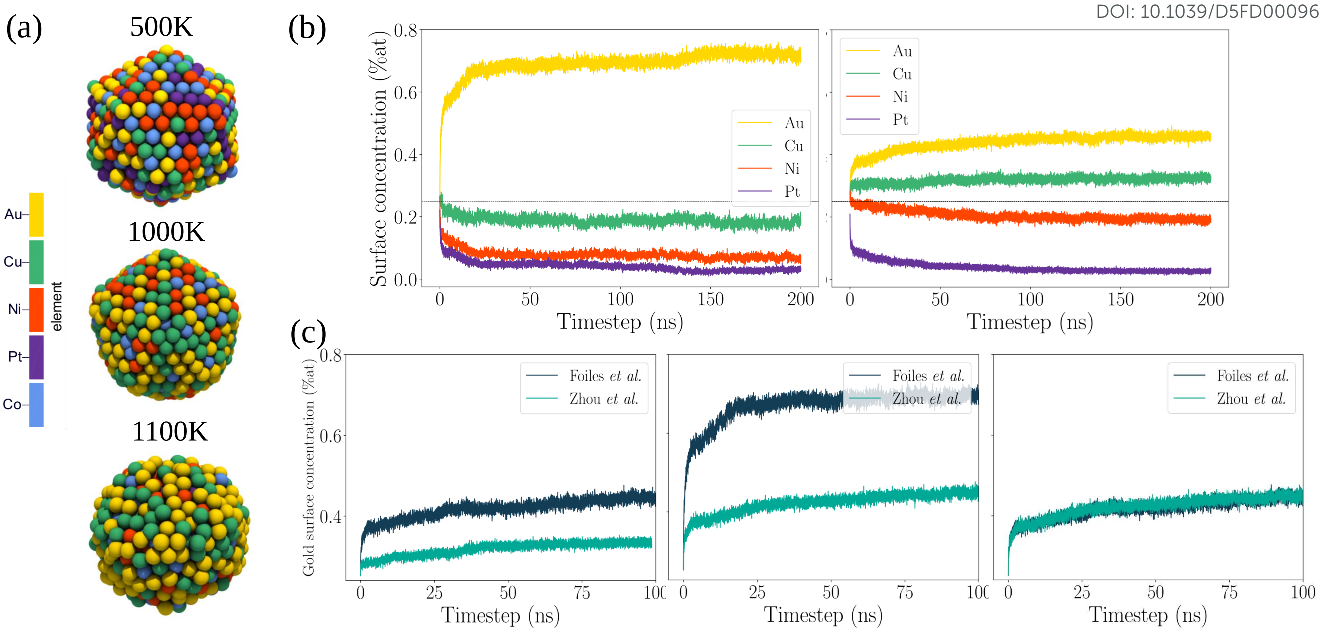

Fig. 1 (a) MD simulations investigating the thermal behaviour of a 3-nm CoNiPtCuAu NP containing 923 atoms in an icosahedral structure. 3D perspective views of the icosahedron shell showing enrichment in Au and Cu at 500, 1000 and 1100 K. (b) Evolution of the surface concentration of all elements in case of an icosahedral HENA containing 3871 atoms at 800 K using the Foiles *et al.* and Zhou *et al.* potentials. (c) Evolution of the Au surface concentration in case of an icosahedral PtNiAuCu NP containing 3871 atoms. Comparison between the two interatomic potentials for different temperatures. From left to right: both potentials at 600 K, both potentials at 800 K, and Foiles potential at 600 K compared with Zhou potential at 800 K.

is well reproduced for all elements, as well as their ratio when compared to DFT calculations. More importantly, the hierarchy among the surface energies of the five elements is perfectly reproduced ($\gamma_{Au} < \gamma_{Cu} < \gamma_{Ni} < \gamma_{Co} < \gamma_{Pt}$) which is crucial to accurately capture the competition between the different elements for segregation.

Furthermore, the study of the thermal stability of NPs also involves knowledge of their solid-liquid transition, which can significantly modify their field of applications and operating conditions. The melting temperature (T_m) is determined by simulated annealing[30], where the typical trend in total energy as a function of temperature is presented in Figure 2a for different sizes of Au NPs. Assuming a crystalline structure, these heat curves exhibit a rapid initial increase in energy as a function of temperature. At the melting point, a sharp jump is observe. This energy jump is indicative of a phase change associated with NP melting. It is followed by a steady rise in energy with temperature as the NP completely liquefies. Using this approach, we determined the melting temperatures T_m of pure metal clusters as a function of particle size (from 309 to 3871 atoms). As shown in Figure 2b, T_m displays a linear decrease as a function of the inverse of particle radius R in agreement with previous works[31]. The radius is obtained by approximating the volume of the icosahedron to the volume of a sphere, using the formula:

$$V = \left(\frac{5(3+\sqrt{5})}{12} \right) l^3 \text{ and } \quad R = \sqrt[3]{\frac{3V}{4\pi}}$$

with l is the length of the edge. From linear extrapolation, a melting temperature of 1143 K is predicted for Au bulk system, in very good agreement with the experimental values of 1337 K. For the other elements, the results of similar analyses are presented in Table 1.

With all the relevant physical parameters of the elements that drive the temperature-driven structural stability of Co-Ni-Pt-Cu-Au systems known, we subsequently assess the driving parameters for the Au and Cu segregation. For this, we first address the thermal stability of the ternary host NPs CoNiPt.

4 CoNiPt NPs

We investigate the structural and chemical evolution of an icosahedral 2057-atom CoNiPt NP (diameter around 4.2 nm) with an equiatomic composition by performing MD calculations over the temperature range from 400 K to 2000 K. Figure 3a presents the final configurations of the particle at different temperatures after numerical convergence is reached. At low temperature (< 900 K), the particle presents a solid crystalline structure, with clearly visible facets and a homogeneous distribution of atoms within the NP and on its surface. Aside from a few atomic rearrangements, the NP structure can be considered stable. When increasing the temperature, the particle maintained its solid state, though a strong enrichment of the surface in Ni can be observed. This is consistent with the surface energy of Ni which is the lowest of the three elements as given in Table 1. Moreover, the cross-sectional view also reveals the presence of Pt atoms in the sub-layer, indicating that the segregation of Ni atoms is accompanied by a depletion of the surface Pt content, which diffuses within

View Article Online
DOI: 10.1039/D5FD00096C

	E_{coh} (eV/atom)	a (Å)	γ (100) (J/m^2)	γ (111) (J/m^2)	T_m (K)
Au	-3.93 (-3.81)	4.08 (4.20)	1.10 (1.63)	0.98 (1.28)	1143 (1337)
Cu	-3.54 (-3.49)	3.61 (3.66)	1.32 (2.17)	1.26 (1.95)	1144 (1358)
Co	-4.40 (-4.39)	3.56 (3.51)	1.73 (2.48)	1.59 (2.04)	1675 (1768)
Ni	-4.45 (-4.44)	3.53 (3.58)	1.51 (2.43)	1.43 (2.01)	1486 (1728)
Pt	-5.77 (-5.84)	3.92 (4.02)	2.18 (2.73)	2.07 (2.30)	1443 (2041)

Table 1 Calculated equilibrium lattice constant (a), cohesion energy (E_{coh}), surface energy (γ) and melting temperature (T_m) for face-centered cubic metals obtained with Zhou *et al.* potential. The experimental and numerical data (quoted in parentheses) used for comparison were obtained from [27–29].

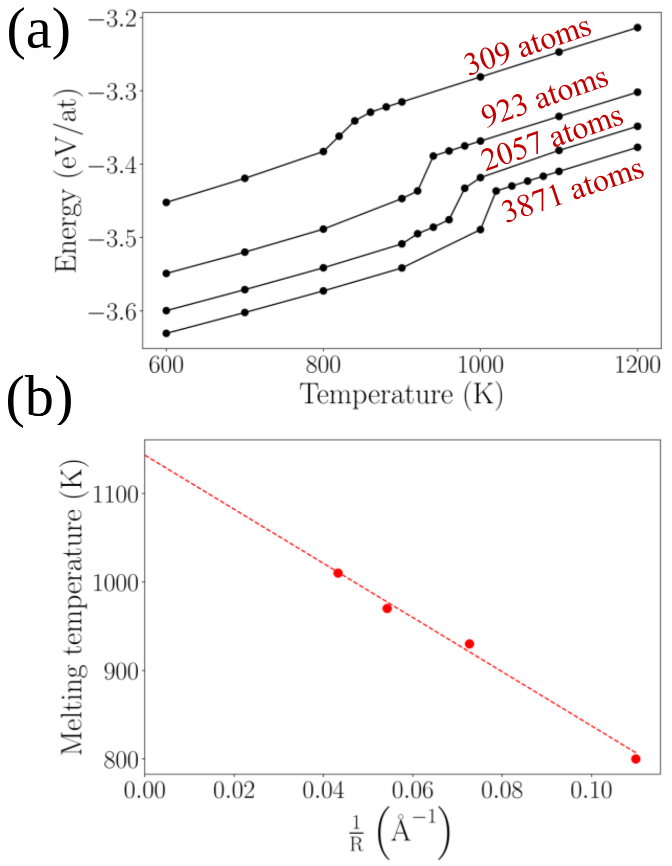

Fig. 2 (a) Total Energy of Au icosahedral nanoparticles of different size as a function of temperature. (b) Evolution of the melting temperature of Au NPs as a function of inverse of the radius ($^{-1}$).

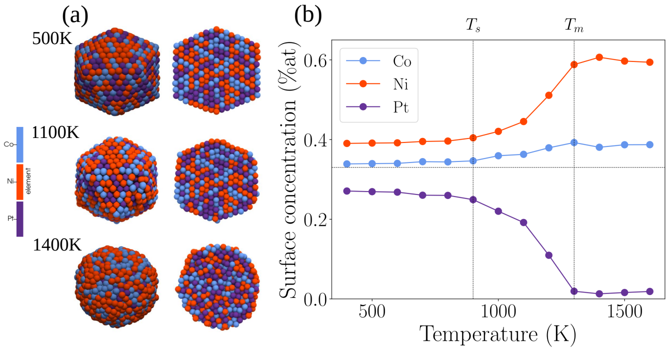

Fig. 3 MD simulations investigating the thermal behavior of a CoNiPt NP in an icosahedral structure containing 2057 atoms a) Equilibrium configurations at different temperatures. The left column presents the shell views and the right one the cross-section views perpendicular to the five-fold axis of the icosahedra. b) Evolution of the surface concentration as a function of the temperature.

the NP. Such a mechanism is not surprising since platinum has the highest cohesive energy and therefore tends to maximize the number of bonds by occupying subsurface sites (see Table 1). At higher temperatures (> 1300 K) when the particle is fully in liquid state, its surface presents a much higher Ni concentration and a complete depletion of Pt. As discussed in the case of the quinary system, three temperature regimes are thus also identified.

To go beyond, the quantitative analysis of the surface concentration of all elements at different temperatures is compared in Figure 3b. As annealing is initiated, atomic rearrangement at surface is activated leading to a slight Ni enrichment at the expense of Pt. As for Co, its surface concentration remains constant at the nominal composition. From a given segregation temperature (marked T_S and here equal to 900 K), a significant change in slope takes place, with a very sharp increase in Ni surface to reach a maximum of around 60 % at 1300 K, together with the complete depletion of Pt. At this temperature, the NP is in liquid state. The surface is predominantly populated by Ni atoms accompanied with slight concentration of Co atoms. Note that the higher presence of Ni on the surface compared to Co is in agreement with theoretical studies on Ni segregation in CoNi particles[32] where the authors specify that the main driving force is the lower surface energy of Ni. As the temperature is further increased, a slight decrease in Ni concentration is predicted, while the concentration of Co and Pt increases very slightly. From MD calculations, it can be concluded that the thermal stability of ternary CoNiPt NPs is affected by the segregation of one element, here Ni, which has the lowest surface energy. Moreover, this phenomenon is thermally activated, since up to a threshold temperature, the surface composition does not vary. At low temperatures, it could be however argued, since diffusion mechanisms are kinetically blocked, that the system is not at thermodynamic equilibrium but is instead trapped in kinetic minimum. To overcome and assess the limitations of MD calculations at low temperature, Monte Carlo (MC) simulations have been also carried out under similar conditions. With the MC

View Article Online
DOI: 10.1039/D5FD00096C

approach, displacement trials coupled with swaps between atoms are more suitable for characterizing the thermodynamic properties of NPs, particularly at low temperatures. Figure 4 presents typical final configurations from MC calculations as well as the evolution of the surface concentration at different temperatures. Clearly, the conclusions differ significantly from MD simulations, particularly for low-temperature regime. Indeed, Ni segregation is significantly enhanced, up to 80% at 400 K. As displayed in Figure 4a, the particle is in the solid state with a surface consisting mainly of Ni atoms. As the temperature increases, the surface Ni concentration decreases in agreement with thermodynamics considerations where superficial segregation can be characterized by segregation isotherms relying the Ni surface concentration to the Ni bulk (or NP core) concentration. Indeed, the main feature of these isotherms is that they are driven by the segregation free enthalpy where the surface concentration of an element is proportional to $\exp(-\Delta G_{seg}/k_B T)$[33,34] and then decreases with increasing temperature. Interestingly, slice views of the atomic models in Figure 4a reveals a Ni core, showing that complete Ni segregation of the surface is combined with equilibrium within the NP. This type of steady-state configuration is very difficult (or even impossible) to capture in MD simulations, where chemical redistribution in the core of the particle is very limited. The equilibrium conditions obtained by MD simulations mainly result from a local equilibrium that takes place via the surface, where atomic diffusion is widely favored. Thus, the analysis using MC simulations enable to show that the results obtained by MD for low temperatures reflect kinetically trapped phenomena, in line with the recent *in situ* TEM measurements on the CoNiPtCuAu HEA NPs.

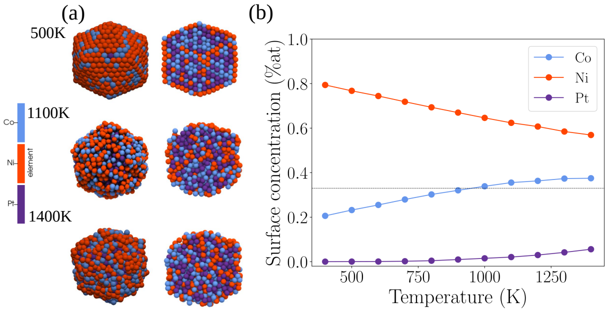

Fig. 4 MC simulations investigating the thermal behavior of a CoNiPt NP in an icosahedral structure containing 2057 atoms. (a) Equilibrium configurations at different temperatures. The left column presents the shell views and the right one the cross-section views perpendicular to the five-fold axis of the icosahedra. (b) Evolution of the surface concentration as a function of the temperature.

The thermal stability of NPs not only concerns segregation phenomena, but also their solid-liquid transition which can significantly impact their conditions of use. As in the case of pure systems, the melting temperature of CoNiPt NPs was therefore determined from calorimetry curves for different particle sizes as shown in Figure 5. Here again, three distinct temperature windows are identified. The first is characterized by a steady increase in total energy with temperature consistent with NPs in the solid state. Then, a slope variation is noted up to a characteristic jump corresponding to the melting temperature, around 1260 K and 1340 K for the NP containing 923 and 2057 atoms, respectively. Finally, the NP is liquid and a gradual increase in total energy is again observed. The analysis of density profiles along the NP radius shown in Figure 6 gives a more quantitative confirmation of these observations and enables further investigation of the solid-liquid transition at the atomic scale. At low temperature (900 K), the radial distribution of elements within the solid NP containing 2057 atoms is characterized by an alternating patterns of peaks, with the three elements fairly homogeneously distributed within the NP.

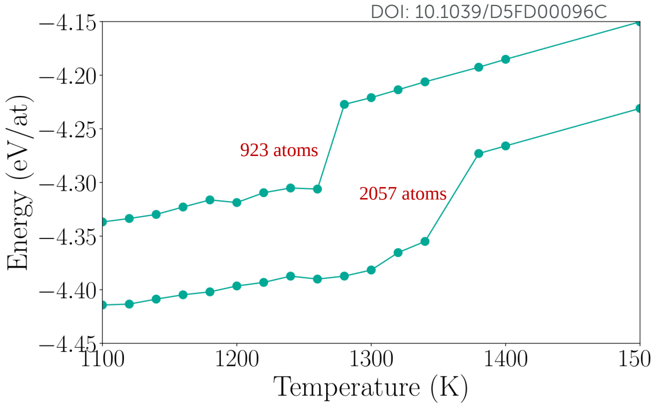

Fig. 5 Total energy (eV/at) as a function of temperature of a CoNiPt NP in an icosahedral structure containing 923 atoms and 2057 atoms.

When the temperature rises to 1200 K, we clearly observe the depletion of Pt at the particle surface, as a result of the migration of Pt atoms to the subsurface layer. At 1330 K, this migration is reinforced with the surface no longer containing any Pt atoms. Moreover, this atomic rearrangement is accompanied by an enrichment of the particle surface with Ni and Co atoms coming from the sub-surface layer. Interestingly, we notice that the peaks associated to the particle surface, as well as those of the second layer, disappear and/or broaden, whereas they remain fairly narrow in the core. Such behavior is indicative of a reduced crystallinity at the surface, the first step towards a transition to the liquid state. Finally, a complete melting of the NP is reached (at T>Tm) where the atomic density distributions show no peak in the particle core, but with high concentrations of Ni and Co at the surface. From this analysis, the solid–liquid transition in case of CoNiPt NP goes through a premelted phase of the surface containing Co and Ni which then propagates along the NP. More precisely, the jump in the calorimetry curve is very abrupt (see Figure 6), corresponding to a first-order transition[35,36]. As for the transformation to the liquid state, it involves melting on one or two layers before propagating directly along the NP, suggesting a partial wetting-type mechanism[37]. Furthermore, it is then tempting to think that such behaviour is driven by the segregated elements. This is confirmed by calculation of the melting temperature of the Co-Ni alloy formed at the particle surface according to Vegard's law of melting points, i.e. taking into account the proportion of elements present on the surface

View Article Online
DOI: 10.1039/D5FD00096C

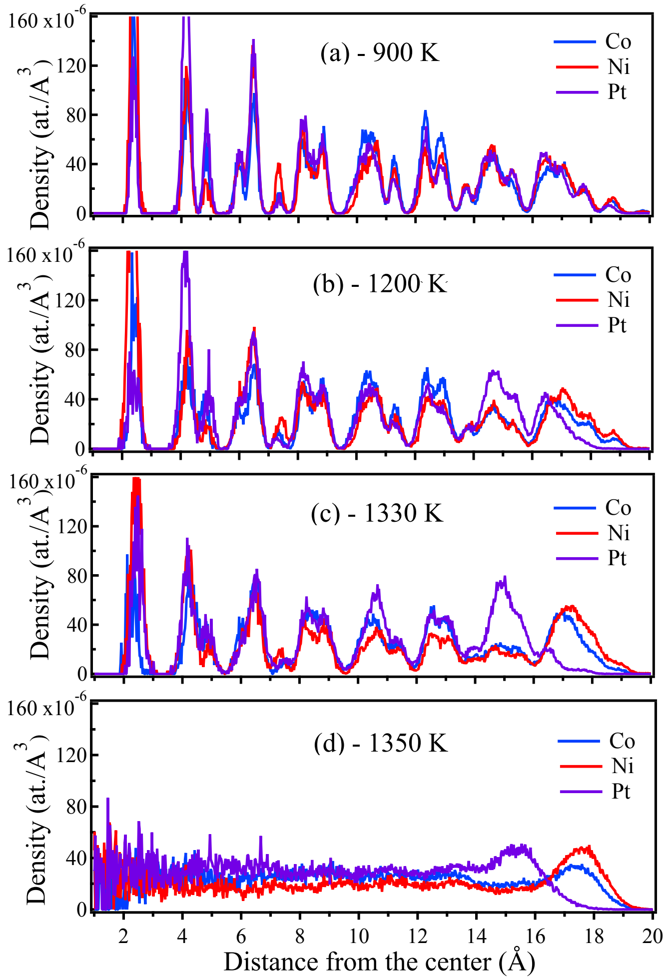

Fig. 6 Atomic density of Co, Ni and Pt as a function of the distance from the center of a CoNiPt NP containing 2057 atoms at (a) 900 K, (b) 1200 K, (c), 1330 K and (d) 1350 K

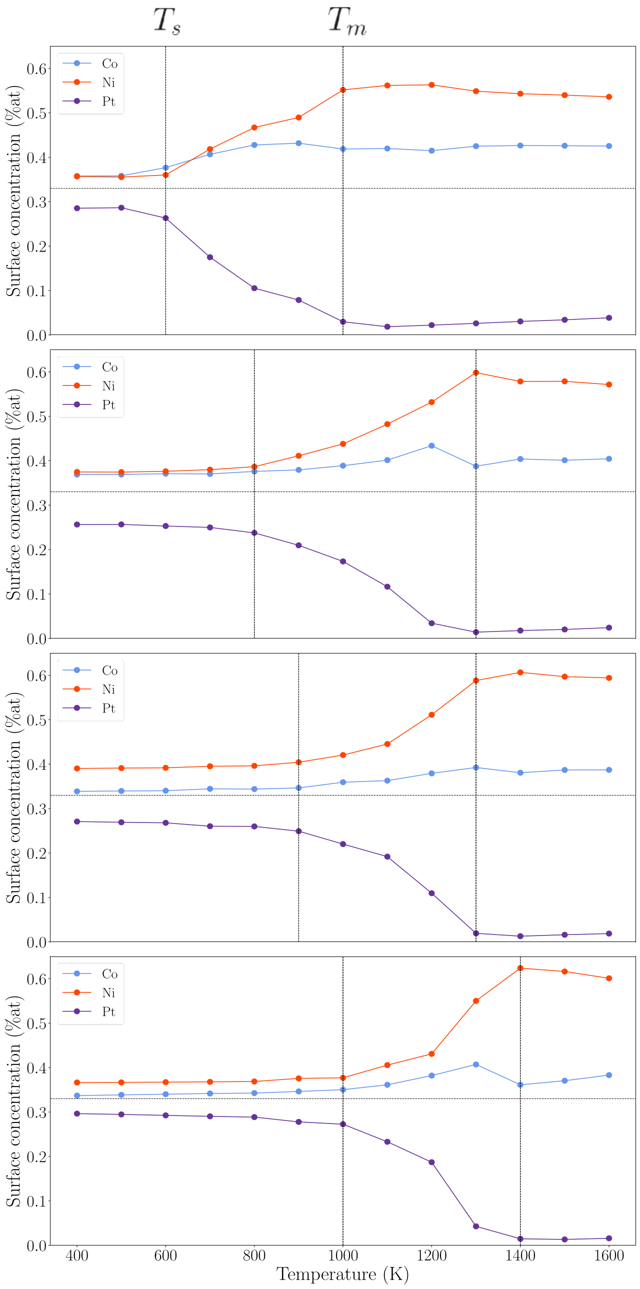

Fig. 7 MD simulations investigating the thermal behavior of a CoNiPt NP in an icosahedral structure containing 309, 923, 2057 and 3871 atoms. Evolution of the surface concentration as a function of the temperature.

View Article Online
DOI: 10.1039/D5FD00096C

and their melting temperatures. As a result, the predicted T$_m$ is about 1368 K in good agreement with the value of 1350 K measured from the calorimetry curve displayed in Figure 5.

Through this detailed study, the thermal stability of a CoNiPt NP containing 2057 atoms was characterized by its melting and segregation temperature. However, these two quantities should vary with size, as usual at the nanoscale where meaningful deviations from bulk properties have been demonstrated for physical quantities such as the melting temperature[31] or the surface energy[38]. To highlight size effect, NPs containing 309 to 3871 atoms were also considered corresponding to sizes of 2.1 to 5.2 nm, respectively. As displayed in Figure 7 the thermal stability increases with the size of the NP. Moreover, both segregation effects and the transition to the liquid state is significantly modified from 600-1000 K to 1000-1400 K when increasing particle size from 309 atoms to 3871 atoms.

5 From ternary to quaternary alloy NPs

We now focus on quaternary alloys where Cu and Au atoms are added to the CoNiPt system. In both cases, the effects on segregation phenomena are striking.

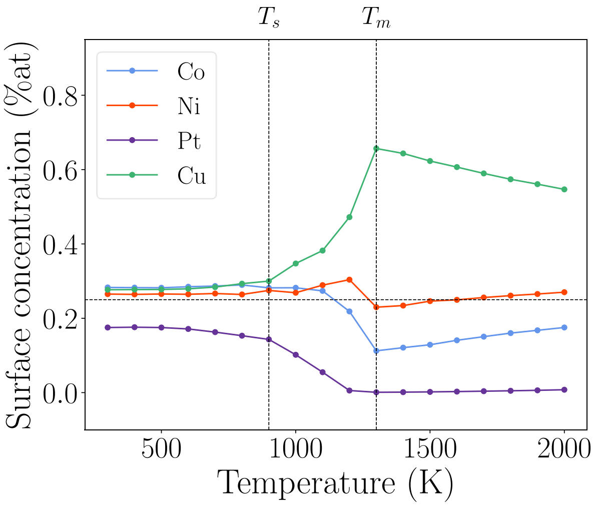

Fig. 8 MD simulations investigating the thermal behavior of a CoNiPtCu NP in an icosahedral structure containing 2057 atoms. Evolution of the surface concentration as a function of the temperature.

To illustrate a typical behaviour of CoNiPtCu NPs, Figure 8 presents the evolution of the surface concentration as a function of the temperature for a NP containing 2057 atoms. The three temperature regimes identified for the ternary and quinary nanoalloys are again observed, though accompanied by a rather singular segregation process. Up to 900 K, an equilibrium situation is established whereby the particle surface is populated with near-equivalent concentrations of Co, Ni and Cu (27 %) which are slightly higher than that of Pt (17 %). The surface then becomes enriched with Cu at the expense of Pt, while Co and Ni concentrations remain stable. When the surface Pt concentration is equal to zero, Cu segregation is reinforced, while Ni and Co diffuse within the NP core. The preferential segregation of Cu at the surface is consistent with the fact that it is the element having both the lowest surface energy and the largest atomic radius. These distinctive physical characteristics leads to a segregation process that occurs more rapidly than in the case of CoNiPt. The same is true for the melting temperature, as Cu is the element with the lowest melting temperature, about 400 K lower compared to Ni and Co.

Hence, the presence of an element such as Cu combining small surface energy, large atomic radius and low melting temperature, is likely to lower the thermal stability of CoNiPtCu NPs. As gold has even more pronounced physical properties in this respect (see Table 1), CoNiPtAu NPs are then expected to exhibit even lower thermal stability as clearly illustrated in the case of a small NP containing 923 atoms. As shown in Figure 9a, segregation mechanisms in this case are activated at very low temperatures (as from 400 K) leading to a surface gold concentration of around 76%. For larger NPs of 2057 atoms, the same phenomenon occurs, with an extremely high surface concentration of gold of the order of 89% (see Figure 9b). Clearly, the presence of gold segregating at the surface with a low melting point is not an ideal condition for sustaining a solid state NP with a homogeneous solid solution. With regard to the solid-liquid transition, it is interesting to note that the calorimetry curve seems to indicate a second-order transition (see Figure 9c).

Analysis of the radial density profiles within the CoNiPtAu NP containing 2057 atoms provides further insight into this physical process (see Figure 10). The initial configuration reveals quite sharp peaks as expected for a crystalline structure with a homogeneous distribution of the elements. As the temperature rises, the surface becomes enriched in Au, at the expense of Pt, which occupies the sub-layer. On the other hand, the distribution associated with Co and Ni does not vary significantly. Above 10 Å, the atomic density profiles display broad peaks indicative of the initiation of a solid-liquid transition. We clearly establish that, while Co and Ni are also present, the surface is strongly enriched in Au and entirely depleted in Pt. As for the two immediate two sub-layers, they consist mainly of Pt and a homogeneous mixture of Ni and Co, with Au being nearly absent. When the solid–liquid transition is reached, at 1100 K, all peaks disappear from the atomic density profiles revealing strong presence of Au atoms at the surface. In contrast to CoNiPt NPs, the solid-liquid transition is smoother, with a complete melting starting at the surface and extending throughout the NP characterized by the continuous evolution of the calorimetry curve typical of a second-order transition (Figure 9b). Finally, based on these findings, the enhanced thermal instability of CoNiPtAu NPs is obvious, as compared to CoNiPtCu NPs. Since gold is the element with the lowest surface energy and the largest atomic radius, it is characterized by two driving forces that greatly favor its segregation at the surface. In addition, when NPs with different gold concentrations are investigated, it appears that the segregation effect is enhanced for gold-enriched NPs demonstrating that varying the atomic composition of each element can impact the segregation behavior. Lastly, Au is the element with the lowest melting point, and so, the solid-liquid transition occurs at relatively low temperature, deviating from

View Article Online
DOI: 10.1039/D5FD00096C

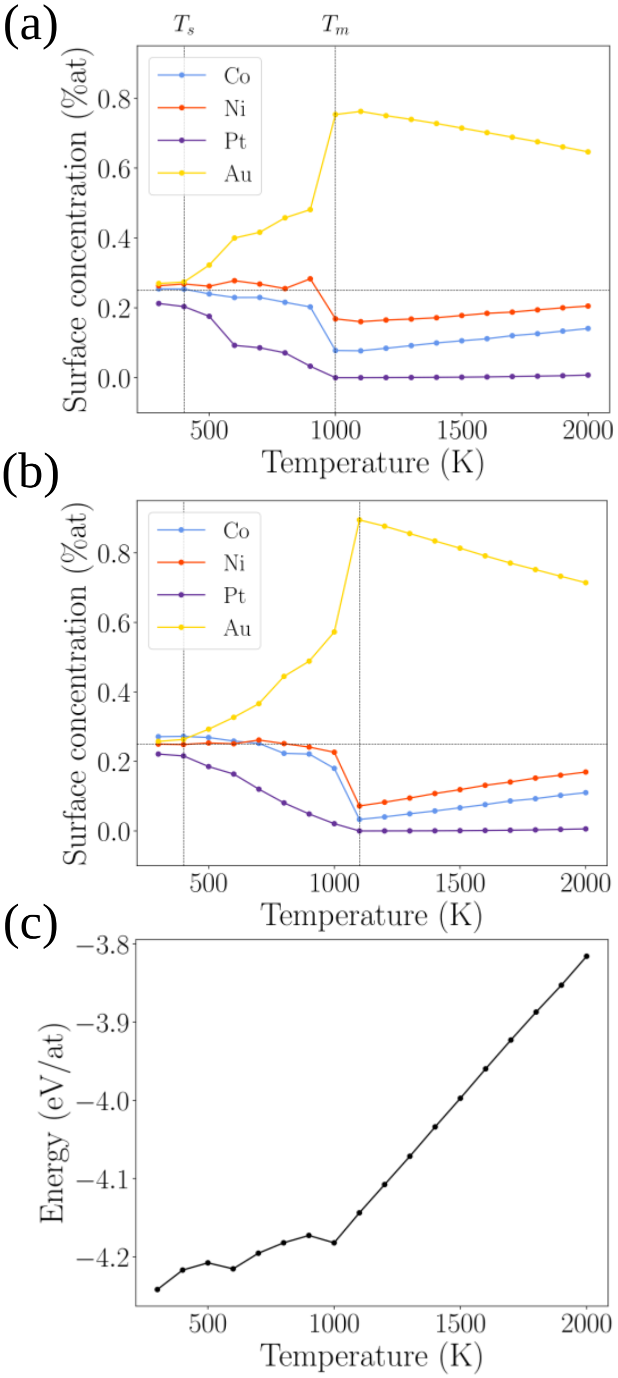

Fig. 9 MD simulations investigating the thermal behavior of a CoNiPtAu NP in an icosahedral structure. Evolution of the surface concentration as a function of the temperature for CoNiPtAu NP containing (a) 923 atoms and (c) 2057 atoms. (b) Total energy (eV/at) as a function of temperature for the NP containing 2057 atoms.

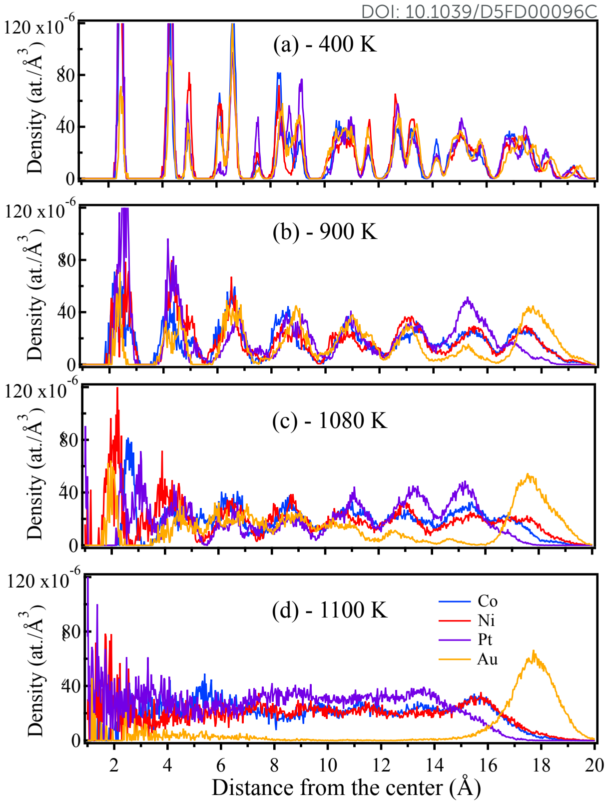

Fig. 10 Atomic density of Co, Ni, Pt and Au as a function of the distance from the center of a CoNiPtAu NP containing 2057 atoms at (a) 400 K, (b) 900 K, (c), 1050 K and (d) 1100 K.

the ideal solid solution structure of HEA NPs with high melting temperature targeted for various applications.

Discussion

Our detailed atomistic study revealed that the presence of Cu and Au atoms have a negative impact on the thermal stabilization of the NPs considered here. To illustrate this point, Figures 11a and b show melting temperatures and temperature segregation ranges for different NP sizes from ternary to quinary alloys. This last information corresponds to the temperature range where significant changes in surface concentration were observed during our simulations. Focusing on the melting temperature, we observe that CoNiPt NPs have the highest melting points at a given NP size. This characteristics results from the low melting temperature of the atoms segregating at the surface, i.e. Co and particularly, Ni atoms. This is confirmed by the estimated T$_m$ derived from Vegard's law, which agree rather well with the values derived from MD calculations. It is clear that for quaternary nanoalloys, the incorporation of Cu and Au reduces the solid-liquid transition as expected, since these two elements which segregate at the surface have the lowest melting points. In the case of the quinary nanoalloys, the evolution of T$_m$ is intermediate between those of the quaternary nanoalloys considered, confirming once again that the presence of both elements at the surface drives the mechanisms of the solid-liquid transition. Regarding the temperature ranges in which segregation occurs, CoNiPt exhibits the highest initial seg-

DOI: 10.1039/D5FD00096C

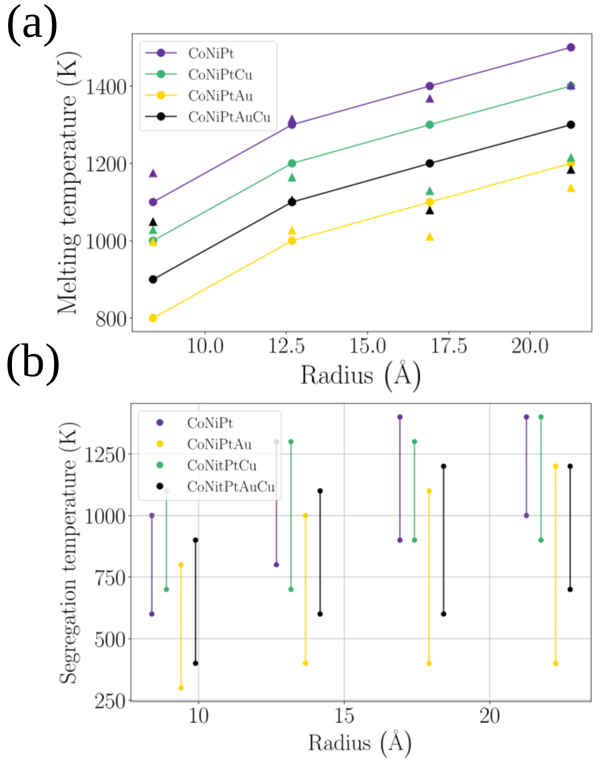

Fig. 11 (a) Melting temperature as function of size for CoNiPt, CoNiPtCu, CoNiPtAu and CoNiPtCuAu NPs. The triangular points correspond to the melting temperature calculated using Vegard's Law. (b) Segregation temperature as function of size for CoNiPt, CoNiPtCu, CoNiPtAu and CoNiPtCuAu NPs.

regation temperature and the narrowest segregation range, all of which stabilize rapidly with increasing particle size (see Figure 11b). In the case of quaternary nanoalloys, the most unfavorable situation is found in the presence of Au atoms, which segregate at the surface at very low temperatures. The temperature range is quite wide, and increases significantly with NP size. Such characteristics are clearly damaging to the stability of HEA NPs. If we consider CoNiPtCuAu NPs, we find an intermediate behaviour with the two quaternary systems considered here, demonstrating once again the importance and crucial role of Au and Cu elements in the properties of these nano-objects.

Conclusion

In the present work, the thermal stability of the HEA NPs is analysed and quantified in terms of melting temperature, as well as segregation mechanisms. On the basis of our work, we can state that to obtain the most stable HEA NP possible, it is preferable to consider systems where the element that will tend to segregate (lowest surface energy and/or largest lattice parameter) has the lowest melting temperature. As discussed in[26], for more simple bimetallic system, it is possible to analyse the contribution and impact of the three effects (the cohesion , the size and the alloying, i.e. the tendency of the alloy to form homo- or hetero-atomic bounds) on segregation phenomena. Therefore, in the case of Cu-Au, which is a system with a strong tendency to order [39], we cannot ignore the fact that the segregation of the two elements within the HEA NP is driven by the high tendency of the system to form Au-Cu bonds. In addition, realistic atmospheric conditions can introduce more complex factors since the surface chemistry can be strongly modified by the interaction of each element with the gaseous molecules. A typical example is the case of Cu-Au binary NPs, where segregation of Au at the surface is observed in vacuum conditions[40] while the atmospheric environment reveals Cu segregation[41]. Such studies imply a detailed analysis of the driving forces, where MC-type simulations coupled to machine learning potentials can be more appropriated. This will be a further step forward to provide a better understanding of the phase stability and transformations of HEA NPs to identify the respective influences of the different driving forces. This in-depth analysis is incredibly complex, as each system is unique, but it is essential to pave the way for rational optimization and design of the phase structures of HEA NPs for application in various fields, particularly at high temperatures.

Conflicts of interest

“There are no conflicts to declare”.

Acknowledgements

This work was supported by ANR YOSEMITE: ANR-22-CE08-0033-01. This study was supported by the IdEx Université Paris Cité (ANR-18-IDEX-0001). H.A. thanks Bernard Legrand for fruitful discussions.

Notes and references

1 B. Cantor, I. T. Chang, P. Knight and A. J. Vincent, *Materials Science and Engineering: A*, 2004, **375-377**, 213–218.

View Article Online
DOI: 10.1039/D5FD00096C

2 J.-W. Yeh, S.-K. Chen, S.-J. Lin, J.-Y. Gan, T.-S. Chin, T.-T. Shun, C.-H. Tsau and S.-Y. Chang, *Advanced Engineering Materials*, 2004, **6**, 299–303.

3 E. P. George, D. Raabe and R. O. Ritchie, *Nature Reviews. Materials*, **4**, year.

4 S. D. Lacey, Q. Dong, Z. Huang, J. Luo, H. Xie, Z. Lin, D. J. Kirsch, V. Vattipalli, C. Povinelli, W. Fan, R. Shahbazian-Yassar, D. Wang and L. Hu, *Nano Letters*, 2019, **19**, 5149–5158.

5 G. Zhang, K. Ming, J. Kang, Q. Huang, Z. Zhang, X. Zheng and X. Bi, *Electrochimica Acta*, 2018, **279**,.

6 S. Dhakar, A. Sharma, N. K. Katiyar, A. Parui, R. Das, A. K. Singh, C. S. Tiwary, S. Sharma and K. Biswas, *Materials Today Energy*, 2023, **37**, 101386.

7 R. Strozi, D. Leiva, J. Huot, W. Botta and G. Zepon, *International Journal of Hydrogen Energy*, 2021, **46**, 2351–2361.

8 S. Nellaiappan, N. K. Katiyar, R. Kumar, A. Parui, K. D. Malviya, K. G. Pradeep, A. K. Singh, S. Sharma, C. S. Tiwary and K. Biswas, *ACS Catalysis*, 2020, **10**, 3658–3663.

9 Y. Yao, Z. Huang, P. Xie, S. D. Lacey, R. J. Jacob, H. Xie, F. Chen, A. Nie, T. Pu, M. Rehwoldt, D. Yu, M. R. Zachariah, C. Wang, R. Shahbazian-Yassar, J. Li and L. Hu, *Science*, 2018, **359**, 1489–1494.

10 F. Waag, Y. Li, A. R. Ziefuß, E. Bertin, M. Kamp, V. Duppel, G. Marzun, L. Kienle, S. Barcikowski and B. Gökce, *RSC Adv.*, 2019, **9**, 18547–18558.

11 A. Barbero, C. Moreira Da Silva, N. O. Peña, N. Kefane, A. Jaffar, M. Thorey, H. Bouaia, J. Nelayah, G. Wang, H. Amara, C. Ricolleau, V. Huc and D. Alloyeau, *Faraday Discussions*, 2022.

12 L. Yang, R. He, J. Chai, X. Qi, Q. Xue, X. Bi, J. Yu, Z. Sun, L. Xia, K. Wang, N. Kapuria, J. Li, A. Ostovari Moghaddam and A. Cabot, *Advanced Materials*, **37**, 2412337.

13 C. Moreira Da Silva, H. Amara, F. Fossard, A. Girard, A. Loiseau and V. Huc, *Nanoscale*, 2022, **14**, 9832–9841.

14 L. Kush, S. Srivastava, Y. Jaiswal and Y. Srivastava, *Materials Research Express*, 2020, **7**, 035704.

15 X. Wang, W. Guo and Y. Fu, *J. Mater. Chem. A*, 2021, **9**, 663–701.

16 S. Krouna, A. Acheche, G. Wang, N. O. Pena, R. Gatti, C. Ricolleau, H. Amara, J. Nelayah and D. Alloyeau, *Advanced Materials*, 2025, **37**, 2414510.

17 F. Calvo, *Phys. Chem. Chem. Phys.*, 2023, **25**, 18439–18453.

18 Z. Zeng, J. Zhao, X. Zhou, J. Li and B. Liang, *Chemical Physics*, 2019, **517**, 126–130.

19 M. Ramírez, A. Prada, F. R. Roco, K. Queirolo, W. Schmidt, F. Corvacho, S. E. Baltazar, J. Rogan and F. J. Valencia, *RSC Adv.*, 2025, **15**, 17695–17705.

20 S. Plimpton, *J. Comput. Phys.*, 1995, **117**, 1–19.

21 X. W. Zhou, R. A. Johnson and H. N. G. Wadley, *Phys. Rev. B*, 2004, **69**, 144113.

22 S. M. Foiles, M. I. Baskes and M. S. Daw, *Phys. Rev. B*, 1986, **33**, 7983–7991.

23 R. Ferrando, J. Jellinek and R. L. Johnston, *Chemical Reviews*, 2008, **108**, 845–910.

24 P. Wynblatt and R. Ku, *Surface Science*, 1977, **65**, 511–531.

25 L. Peng, E. Ringe, R. P. Van Duyne and L. D. Marks, *Phys. Chem. Chem. Phys.*, 2015, **17**, 27940–27951.

26 J. Creuze, H. Guesmi, C. Mottet, B. Zhu and B. Legrand, *Surface Science*, 2015, **639**, 48–53.

27 L. Vitos, A. V. Ruban, H. L. Skriver and J. Kollár, *Surface Science*, 1998, **411**, 186–202.

28 C. Kittel, *Introduction to Solid State Physics*, Wiley, Hoboken, NJ, 8th edn, 2005.

29 R. Tran, Z. Xu, B. Radhakrishnan, D. Winston, W. Sun, K. A. Persson and S. P. Ong, *Scientific Data*, 2016, **3**, 160080.

30 A. Front, D. Oucheriah, C. Mottet and H. Amara, *Faraday Discuss.*, 2023, **242**, 144–159.

31 P. Buffat and J.-P. Borel, *Phys. Rev. A*, 1976, **13**, 2287–2298.

32 R. Jayaganthan and G. Chow, *Materials Science and Engineering: B*, 2002, **95**, 116–123.

33 F. L. Williams and D. Nason, *Surface Science*, 1974, **45**, 377–408.

34 J. Creuze, F. Berthier, R. Tétot and B. Legrand, *Surf. Sci.*, 2004, **553**, 168–180.

35 A. G. Khachaturyan, *A. G. Khachaturyan*, Wiley, New York, 1983.

36 F. Ducastelle, *F. Ducastelle*, North Holland, Amsterdam, 1991, vol. 3, pp. 1–49.

37 A. C. Levi and E. Tosatti, *Surface Science*, 1987, **189-190**, 641–644.

38 H. Amara, J. Nelayah, J. Creuze, A. Chmielewski, D. Alloyeau, C. Ricolleau and B. Legrand, *Phys. Rev. B*, 2022, **105**, 165403.

39 H. Okamoto, D. Chakrabarti, D. Laughlin and T. Massalki, *JPE*, 1987, **8**, 454–474.

40 G. Breyton, H. Amara, J. Nelayah, J. Creuze, H. Guesmi, D. Alloyeau, G. Wang and C. Ricolleau, *Phys. Rev. Lett.*, 2023, **130**, 236201.

41 Q. Wang, A. Nassereddine, D. Loffreda, C. Ricolleau, D. Alloyeau, C. Louis, L. Delannoy, J. Nelayah and H. Guesmi, *Faraday Discuss.*, 2023, **242**, 375–388.

View Article Online
DOI: 10.1039/D5FD00096C

Dr. Hakim Amara
Tel: 00 33 1 46 73 48 90
Mail: hakim.amara@onera.fr

Châtillon, 2nd June 2025

Dear Editor,

No new data were created or analysed during this work. Consequently, data sharing is not applicable to this article.

Thank you very much for your consideration of our work.
Sincerely Yours, on the behalf of all the authors,

Dr Hakim Amara

Laboratoire d’Etude des Microstructures – UMR104 – ONERA/CNRS
ONERA – 29 avenue de la Division Leclerc – 92322 Châtillon, France
https://lem.onera.cnrs.fr